3 (2026) 100226

Contents lists available at ScienceDirect

The EANM Journal

journal homepage: www.sciencedirect.com/journal/the-eanm-journal

Multicenter [^{18}F]PI-2620 PET for in vivo staging of tau pathology in progressive supranuclear palsy: a subtype/stage inference algorithm study

Michael Rullmann [a,*,1], Dylan Henssen [a,b,1], Matthias Brendel [c,d,e,1], Jost-Julian Rumpf [f], Johannes Levin [d,e,g], Robert Perneczky [h], Solveig Tiepolt [a], Marianne Patt [a], Andreas Schildan [a], Andre Mueller [i], Victor L. Villemagne [j], Joseph Classen [f], Andrew W. Stephens [i], Stamatia Karagianni [c,d,e], Nicolai Franzmeier [c,d,e], Gabor G. Kovacs [k], Guenter U. Hoeglinger [d,e,g], Osama Sabri [a,1], Henryk Barthel [a,l,1], for the German Imaging Initiative for Tauopathies (GII4T)

[a] Department of Nuclear Medicine, University of Leipzig, Leipzig, Germany
[b] Department of Medical Imaging, Radboud University Medical Center, Nijmegen, Netherlands
[c] Department of Nuclear Medicine, University Hospital of Munich, LMU Munich, Munich, Germany
[d] Munich Cluster for Systems Neurology (SyNergy), Munich, Germany
[e] German Center for Neurodegenerative Diseases (DZNE), Munich, Germany
[f] Department of Neurology, Leipzig University Medical Center, Leipzig, Germany
[g] Department of Neurology, LMU Hospital, Ludwig-Maximilians-Universität (LMU), Munich, Germany
[h] Department of Psychiatry and Psychotherapy, University Hospital, LMU Munich, Munich, Germany
[i] Life Molecular Imaging GmbH, Berlin, Germany
[j] Department of Psychiatry, University of Pittsburgh, Pittsburgh, USA
[k] Department of Laboratory Medicine and Pathobiology, University of Toronto, Toronto, Canada
[l] Department of Nuclear Medicine, Municipal Hospital Dessau, Dessau, Germany

ARTICLE INFO

Keywords:
Progressive supranuclear palsy
PI-2620
Tau PET
SuStaIn

ABSTRACT

Progressive supranuclear palsy (PSP) is a primary 4R tauopathy. Postmortem studies identified six tau pathological stages with tau aggregation with involvement of the subthalamic nucleus and the globus pallidus, with further affliction of the striatum, cerebellum with dentate nucleus, frontal and/or occipital cortices. We aimed to test whether this staging system is also observed when an unsupervised machine learning model is used to analyze in vivo [^{18}F]PI-2620 tau PET imaging data. Furthermore, regional differences in tau tracer binding in different PSP subtypes and corresponding clinical profiles were investigated.

Methods: We analyzed imaging and clinical data of 120 patients with the clinical diagnosis of PSP and of 16 healthy controls. Dynamic [^{18}F]PI-2620 PET imaging in a multicenter setting (sites in Germany and Australia) was performed over 60min. After kinetic modeling, parametric distribution volume ratio images were analyzed and classified into different pattern subtypes and stages by use of the SuStaIn algorithm. Regional differences in tau tracer binding were assessed using statistical parametric mapping.

Results: The SuStaIn model distinguished three patterns of [^{18}F]PI-2620 binding: i) a subcortical pattern, ii) a rhombencephalic pattern, and iii) a cortical pattern. The subcortical pattern showed a spatiotemporal distribution similar to the previously published PSP postmortem staging system. Subjects in different SuStaIn-derived patterns showed different clinical characteristics, including a significant association with sex ($P < 0.001$).

Conclusion: These results provide motivation to further develop [^{18}F]PI-2620 as an imaging biomarker of PSP. They also demonstrate the potential of the SuStaIn model to reveal so-far-unknown tau tracer binding patterns in PSP, with possible implications for improved phenotyping and future anti-tau treatment decisions.

* Corresponding author. Liebigstr. 18, 04103, Leipzig, Germany.
E-mail address: rullmann@medizin.uni-leipzig.de (M. Rullmann).
[1] These authors contributed equally to this work.

https://doi.org/10.1016/j.eanmj.2026.100226
Received 12 March 2026; Received in revised form 29 April 2026; Accepted 7 May 2026
Available online 20 May 2026

List of abbreviations

4R = 4-repeat
AAL = Automated Anatomical Labeling
CBS = Corticobasal syndrome
CVIC = Cross-validation information criterion
DVR = Distribution volume ratio
MCMC = Markov Chain Monte Carlo
MNI = Montreal Neurological Institute
MoCA = Montreal Cognitive Assessment
MRI = Magnetic resonance imaging
MRTM2 = Multilinear reference tissue model 2
OSEM = Ordered subset expectation maximization
PET = Positron emission tomography
PSP = Progressive supranuclear palsy
PSP-CBS = Progressive supranuclear palsy–corticobasal syndrome
PSP-FTD = Progressive supranuclear palsy–frontotemporal dementia
PSP-P = Progressive supranuclear palsy–parkinsonism
PSP-PAGF = Progressive supranuclear palsy–pure akinesia with gait freezing
PSP-RS = Progressive supranuclear palsy–Richardson syndrome
PSP-SL = Progressive supranuclear palsy–speech/language variant
PSPRS = Progressive supranuclear palsy rating scale
SEADL = Schwab and England Activities of Daily Living Scale
SPM = Statistical parametric mapping
SPM12 = Statistical Parametric Mapping version 12
SuStaIn = Subtype and Stage Inference
SUVR = Standardized uptake value ratio
VOI = Volume of interest

1. Introduction

Progressive supranuclear palsy (PSP), a severe, progressive form of atypical parkinsonism, is classified as a primary tauopathy. Tauopathies form a spectrum of disorders in which intracellular (i.e., neuronal, oligodendroglial and astrocytic) aggregation of microtubule-associated protein tau occurs. Depending on the alternative splicing of the exon, different isoforms of tau with different numbers of repeats can be encountered. In PSP, the 4-repeat (4R) isoform of tau is found. PSP, however, is not the only 4R tauopathy, as intracellular accumulation of this isoform of tau is also observed in corticobasal degeneration, argyrophilic grain disease and globular glial tauopathy. It is generally accepted that the distribution and severity of 4R-tau accumulation dictates the clinical symptomatology and thus defines the disease entity. Different tau accumulation patterns and sequences might explain why PSP patients may represent with a variety of cognitive and motor symptoms [1,2]. Eight phenotypical patterns of PSP have been described in the available literature. The most commonly encountered phenotypical category of PSP patients concerns the PSP-Richardson syndrome (PSP-RS). These patients present with early postural instability and oculomotor dysfunction (e.g., abnormal vertical saccades and supranuclear gaze palsy) accompanied by behavioral and personality changes and executive dysfunction. When patients present with other predominant features, such as parkinsonism, pure akinesia with gait freezing, corticobasal syndrome features, speech and language dysfunction or predominant frontotemporal dysfunction, a clinical phenotype of PSP-P, PSP-PAGF, PSP-CBS, PSP-SL and PSP-FTD, respectively, is diagnosed [3]. These different phenotypical PSP subtypes are sometimes difficult to disentangle and to diagnose on clinical grounds. They are, however, without exception, severe, progressive, and currently not curable. In PSP, the search for improved biomarkers is ongoing with high intensity, with tau PET imaging being a promising candidate. Since the development of the second-generation tau tracers, more specific tracer binding to 4R tau and, therefore, more accurate diagnostic imaging of PSP has become possible [4–6]. A 2023 meta-analysis of Jin et al. [7] reported that topographic tau burden was different between PSP patients and healthy controls when analysing a variety of tracers (i.e., [^{18}F]AV-1451, [^{18}F]THK-5351, [^{11}C]PBB3, [^{18}F]PI2620, [^{18}F]PM-PBB3 and [^{18}F]FDDNP). They reported that tau accumulation was higher in the red nucleus, subthalamic nucleus and globus pallidus in PSP-RS patients compared to PSP-P patients [7]. However, no differences in regional tracer uptake between the other different phenotypical variants of PSP in any other brain region were observed [7]. This shows the complexity of PSP subtype discrimination which can be possibly explained by co-existing temporal and phenotypic heterogeneity [8]. On the other hand, different tracers are known to have different affinity profiles to 4R-tau, with [^{18}F]PI2620 being the most promising radioligand [4,9], and this could have influenced meta-analysis findings.

In another study, [^{18}F]Florzolotau PET images were analyzed by an unsupervised machine learning, Subtype and Stage Inference (SuStaIn), algorithm. The SuStaIn algorithm was able to define two distinct tracer binding pattern-based subtypes in PSP [10], showing its ability to model both limitations simultaneously. SuStaIn is a probabilistic unsupervised machine-learning algorithm in which phenotypical heterogeneity (i.e., disease type) and temporal progression (i.e., disease stage) are deduced. Although subtype 1 was characterized by a rapidly spreading, subcortical-to-cortical progression of tau accumulation, resulting in more severe neurological deficits, it remained largely elusive how these two subtypes correlated with histopathological findings and clinical PSP phenotypes.

Therefore, this study investigated the capacity of the SuStaIn algorithm to discover tracer binding-related subtypes of PSP patients when using [^{18}F]PI-2620 PET. The validity of the discovered SuStaIn-derived PSP subtypes was tested against the known histopathological PSP tau staging system as reported by Kovacs et al. [11].

2. Materials and methods

2.1. Ethical statement

The ethics committee of the Ludwig-Maximilians-University Munich and of the University of Leipzig (ethical review board assigned file number 17-569 (approved 24-10-2017) and 19-022 (approved 22-10-2019), respectively) approved the study according to the Declaration of Helsinki. All participants provided written informed consent prior to undergoing the [^{18}F]PI-2620 PET session.

2.2. Inclusion of patients and healthy controls

Patients with a clinical diagnosis of a phenotypical variant of PSP were eligible for inclusion. Age, sex, disease duration and symptom severity were collected at the moment of inclusion. Final diagnosis followed international diagnostic criteria [12] by board certified neurologists at the University of Leipzig or Ludwig-Maximilians-University Munich.

The healthy control cohort (n = 16) was derived from two centers: The Ludwig-Maximilians-University Munich provided data from 11 individuals (mean age of 71.7 ± 11.3 years, 4 females). The University of Melbourne, Australia contributed data from five individuals (mean age of 69.4 ± 7.6 years, all female).

2.3. Clinical data

PSP symptom severity was evaluated using the PSP rating scale [13].

Severity of symptomatology was also assessed using the Schwab and England Activities of Daily Living Scale (SEADL) [14]. Cognitive status was evaluated by the Montreal Cognitive Assessment (MoCA) [15].

2.4. [^{18}F]PI-2620 PET imaging

Radiosynthesis of [^{18}F]PI-2620 followed published procedures [16]. This multicenter study included data from three centers: Ludwig-Maximilians-University Munich, Germany, University of Melbourne, Australia, and University of Leipzig, Germany. Dynamic acquisitions were performed in 3D list mode for 60 min post-injection of ~185 MBq [^{18}F]PI-2620.

PET data in Munich were acquired on Siemens Biograph TruePoint 64 PET/CT or Siemens mCT systems. Dynamic brain PET was recorded in 3D list mode for 60 min and reconstructed using OSEM (4 iterations, 21 subsets, 5 mm Gaussian filter) into a 336 × 336 × 109 matrix (voxel size 1.02 × 1.02 × 2.03 mm^3), with low-dose CT attenuation correction.

In Leipzig, PET data were acquired on a Biograph mMR PET/MR system using 3D list-mode over 60 min and reconstructed with OSEM (8 iterations, 21 subsets, 3 mm Gaussian filter) into a 256×256 matrix (1.00 × 1.00 × 2.03 mm^3 voxel size); HiRes attenuation correction was applied.

In Melbourne, dynamic brain PET (0–60 min) was acquired on a Philips Gemini TF 64 PET/CT and reconstructed with LOR-RAMLA and CT attenuation correction into a 128 × 128 × 89 matrix (2.00 × 2.00 × 2.00 mm^3 voxel size).

2.5. PET data post-processing

Dynamic PET data were motion-corrected in PMOD (PMOD Technologies LLC, Zurich, Switzerland) and co-registered with individual T1-weighted MRIs when available. Parametric distribution volume ratio (DVR) maps, serving as tau load estimates, were generated using a multilinear reference tissue model (MRTM2), with the lower cerebellum (excluding dentate nucleus) as reference [17].

For statistical parametric mapping (SPM12, Wellcome Trust Centre for Neuroimaging, London, UK), DVR maps were spatially normalized to MNI space using the T1-weighted MRI when available otherwise based on early PET images (n = 24, 0-15 min p.i.) and its corresponding template, then smoothed with an 8 mm Gaussian kernel.

For volume-of-interest (VOI) analyses, AAL, Basal Ganglia, and SUIT atlases [18–20] were non-linearly transformed to individual space using the inverse MNI spatial transformation. PET statistics were extracted from regions relevant for PSP histopathological staging [11]: globus pallidus (Basal Ganglia), subthalamic nucleus (Basal Ganglia), striatum (Basal Ganglia), frontal cortex (AAL), dentate nucleus (SUIT) and cerebellar white matter (AAL), and occipital cortex (AAL) [11,21]. The DVR values in these regions of interest were used as the input for the SuStaIn model.

2.6. SuStaIn modelling

Subtype and Stage Inference (SuStaIn) models biomarker progression using event-based linear z-score modeling [8,22]. It assumes continuous accumulation of biomarkers—in this case, tau PET readouts—and estimates subtype category, trajectory, and posterior probabilities. Subtypes are identified hierarchically using expectation–maximization, iterating between updating subtype progression sequences and the fraction of patients assigned to each subtype. Subtype 0 in the SuStaIn framework represents individuals without detectable abnormality in the modelled features (all stage 0 individuals). Therefore, Subtype 0 or the stage 0 subgroup holds no changes that are informative for subtype or stage inference. This does not indicate that the individuals are healthy; it implies that the individuals in this Subtype cannot be clustered based on the given input data.

Input included DVR z-scores (adjusted for age, sex, and center) for each VOI, control-derived cut-offs, maximum adjusted z-scores, and SuStaIn hyperparameters: maximum 3 subtypes, 25 random initializations, and 100,000 MCMC iterations [8,23]. The adjusted z-scores were calculated following a normative modeling framework: we used ordinary least squares regression to define the expected VOI values based on the control group, subsequently calculating adjusted z-scores to quantify each participant's deviation from these age-, sex-, and site-adjusted norms.

Optimal subtype number was determined using cross-validation information criteria (CVIC) and log-likelihood histograms, validated by 10-fold cross-validation. Subtype progression patterns across folds were compared to assess consistency. Fig. 1 summarizes the methodology of this paper.

2.7. SuStaIn output

SuStaIn outputs were visualized with positional variance diagrams, displaying VOI-specific [^{18}F]PI-2620 binding (vertical axis) over disease progression (horizontal axis). Color-coded certainty levels highlighted probabilities of VOIs reaching z-thresholds (red, magenta, blue for increasing severity).

2.8. Statistical parametric mapping

Group-level voxel-wise comparisons were performed in SPM12 using two-sample t-tests between PSP patients and controls to assess differences between SuStaIn-derived subtypes. Results were thresholded at $p < 0.001$. For cortical regions, a minimum cluster size of 30 voxels was required, while subcortical analyses used no cluster size threshold due to smaller volumes.

2.9. Tau PET PSP staging methodology

DVR maps from healthy controls were used to compute z-scores within VOIs derived from Kovacs et al. [11]. Abnormal tau binding was stratified at thresholds of z = 1 (+, limited), z = 2 (++, mild), and z = 3 (+++, moderate/severe) [10]. Based on the staging scheme by Kovacs et al. [11], PSP progression was stratified into six stages: Stage 1, involvement of subthalamic nucleus, globus pallidus, or striatum; Stage 2, simultaneous involvement of these regions; Stage 3, additional cerebellar (non-dentate) or frontal involvement; Stage 4, all Stage 3 regions affected; Stage 5, occipital limited involvement; and Stage 6, occipital moderate/severe involvement. For each participant, an in vivo stage was assigned by determining the highest stage for which the corresponding regions showed different degrees of tracer uptake (using the aforementioned z-score thresholds reflecting increasing levels of involvement), following the hierarchical structure of the Kovacs staging scheme [11].

2.10. Statistical analyses

Analyses were conducted with SPSS (v28, IBM, Armonk, NY). Normality was tested using Kolmogorov–Smirnov. For normally distributed data, values were reported as mean ± SD; otherwise, they were reported as median and range. Nominal demographic comparisons between SuStaIn-derived subtypes used ANOVA or Kruskal–Wallis tests depending on distribution, and chi-square tests for categorical data (e.g., sex, PSP phenotype). Correlations between clinical measures (disease duration, PSP rating scale, MoCA, SEADL) and tau patterns were examined with Pearson's correlation. If SuStaIn-derived subtypes aligned with the Kovacs et al. [11] histopathological scheme, corresponding stage correlations were computed, comparing PET-based staging with neuropathological stages using Pearson's correlation. Significance was set at $p < 0.05$. Bonferroni correction was applied for post-hoc analyses.

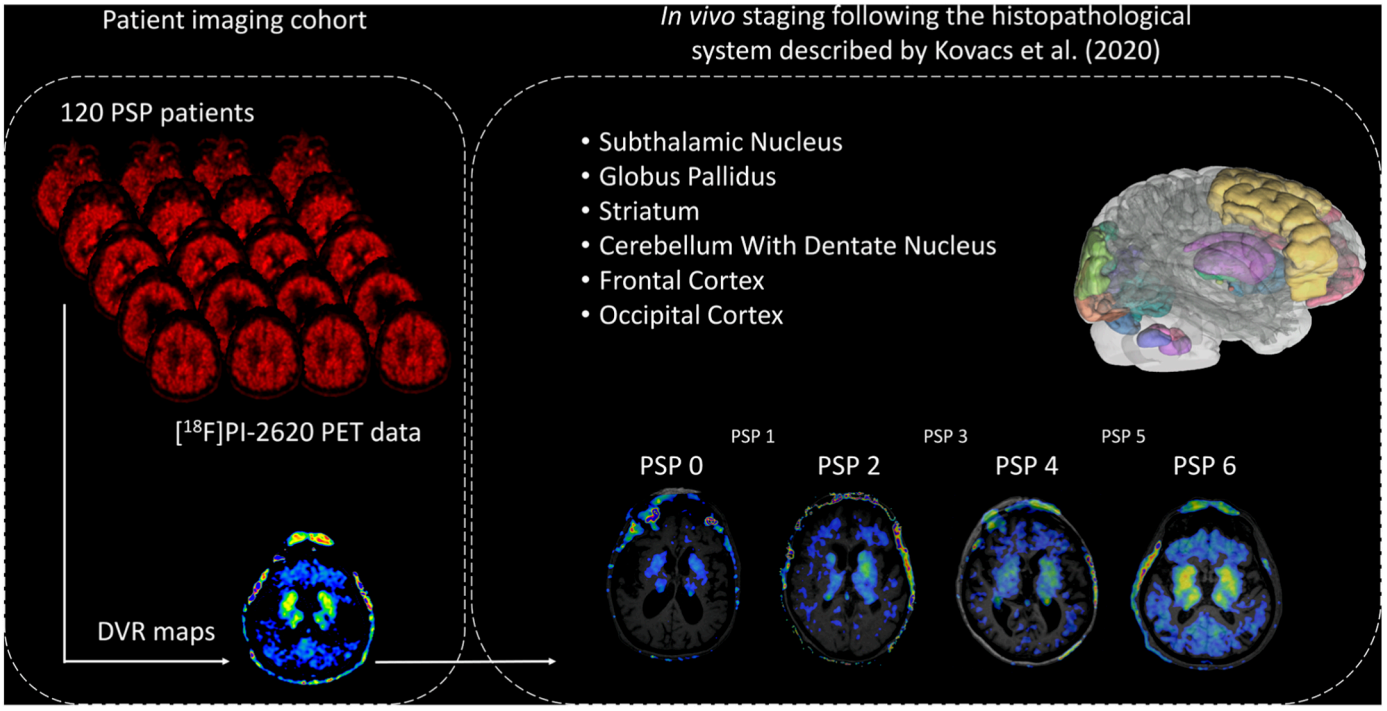

Fig. 1. Schematic representation of methodology and SuStaIn results regarding subtype differentiation. The [^{18}F]PI2620 PET data from 120 subjects were collected, motion-corrected and further post-processed to provide information on tau tracer binding (i.e., DVR maps). Region of interest analysis provided information on tau tracer binding in brain regions known to be involved in PSP following histopathological examination[11,21]][Following the ex vivo methodology presented by Kovacs et al., all cases were staged in vivo.

3. Results

3.1. Demographics

In total, 120 PSP patients (62 males, mean age 72.2 ± 7.0 years) and 16 sex- and age-matched healthy participants (7 males, mean age 71.0 ± 10.1 years) were included in this study (Table 1). Most patients met the criteria for the clinical phenotype of PSP-RS (n = 63), followed by PSP-CBS (n = 16), PSP-P (n = 12), PSP-SL (n = 5), PSP-FTD (n = 5), and PSP-PAGF (n = 1) phenotypes. The PSP patients had a median disease duration of 36 months (range 3.0 - 144.0 months). In the PSP patients, the median PSP rating scale, SEADL and MoCA scores were 30 (range: 9-71), 60 (range: 10-90), and 22 (range: 0-30) points, respectively.

3.2. SuStaIn recognizes three distinct spatiotemporal PSP tau tracer binding subtypes

SuStaIn provided three different tau tracer binding patterns of PSP which could be differentiated by their spatiotemporal evolution in 18 stages, which are defined based on the number of included biomarkers (six VOIs) and the three defined z-score thresholds: z = 1 (+, limited), z = 2 (++, mild), and z = 3 (+++, moderate/severe). While a model with four subtypes could not distinguish all subtypes (CVIC: 3525 vs. 3358 vs. 3346 vs. 3343; log-likelihood: −176 vs. −167 vs. −166 vs. −166), the three-subtype model provided sufficient quality (CVIC: 3534 vs. 3372 vs. 3355; log-likelihood: −176 vs. −168 vs. −166). We named these three different tau tracer binding patterns after the regions of early involvement: the classical subcortical, the rhombencephalic and the cortical pattern. All subjects who, regardless of any further tau tracer binding pattern, were classified as stage 0 (n = 29) were excluded from further analyses. This SuStaIn stage 0 subgroup included almost all healthy controls (n = 14), four patients with the clinical phenotype of PSP-RS, eleven with the phenotype of PSP-CBS, and one with the clinical phenotype of PSP-FTD, PSP-PAGF and PSP-P each (Fig. 2).

The first pattern, containing 62 patients, was named the classical subcortical pattern. This group showed an early involvement of the striatum and globus pallidus, followed by tau PET signals in the

Table 1
Demographics and clinical symptom scores of the PSP patients classified by their clinical phenotype.

	PSP total (n = 120)	PSP-RS (n = 67)	PSP-CBS (n = 27)	PSP-F (n = 6)	PSP-P (n = 13)	PSP-SL (n = 5)	PSP-PGF (n = 2)	Healthy Controls
Age (years)	72.3 ± 7.0	72.1 ± 6.7	71.9 ± 8.3	67.5 ± 4.1	75.5 ± 6.1	75.4 ± 6.2	69.5 ± 10.6	71.0 ± 10.1
Sex (F:M)	54:66	28:39	15:12	4:2	5:8	1:4	1:1	9:7
Disease duration (months)	42.3 ± 30.9	42.5 ± 27.9	35.5 ± 30.9	34.8 ± 37.9	68.4 ± 44.3	31.3 ± 18.1	95.0[a]	-
MoCA score	21.4 ± 5.8	20.8 ± 6.9	21.6 ± 5.9	20.5 ± 6.4	24.2 ± 3.4	24.6 ± 1.2	20.0[a]	-
SEADL score	56.9 ± 19.0	54.8 ± 19.6	57.3 ± 18.8	66.0 ± 18.2	56.7 ± 18.6	70.0 ± 20.0	60.0[a]	-
PSPRS score	33.8 ± 13.6	37.4 ± 13.7	29.2 ± 13.3	26.6 ± 8.3	35.8 ± 11.6	27.3 ± 13.6	17.0[a]	-

MoCA = Montreal Cognitive Assessment questionnaire; PSPRS = Progressive supranuclear palsy rating scale; SEADL = Schwab and England Activities of Daily Living Scale.
[a] = Only one patient due to missing data for one patient.

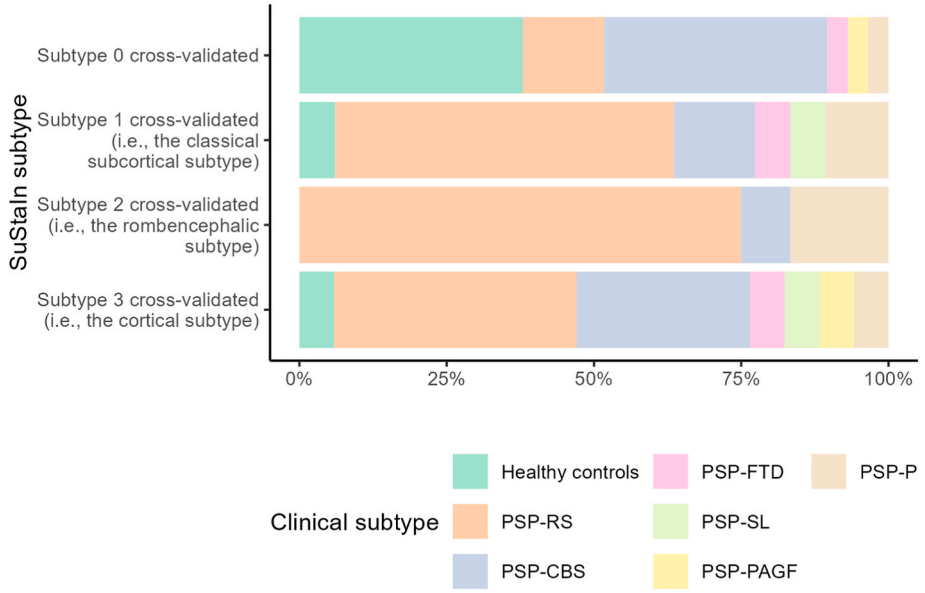

Fig. 2. Barplots showing assignment of clinical subtypes of each SuStaIn subtype.

subthalamic nucleus. In later stages, the cerebellar white matter and dentate nucleus were involved, although severe cerebellar tau tracer binding was only seen in the last stages. Frontal and occipital involvement in this subtype of PSP was seen in later stages as well (Fig. 3A). The second subgroup showed a rhombencephalic pattern (n = 24) and showed more diffuse accumulation of tau, again starting at the subcortical structures prior to affecting the cortical regions. In this rhombencephalic subtype, however, we observed an early stage involvement of the cerebellar white matter and dentate nucleus, the subthalamic nucleus and globus pallidus, getting more pronounced over the course of multiple stages. Cerebellar involvement was followed by tau accumulation in the striatum in later stages. At the end stages of this rhombencephalic subgroup, cortical involvement was observed with similar onset and pattern in the frontal and occipital lobes (Fig. 3B). The third pattern, the cortical subtype, included 17 patients and showed involvement of the occipital and frontal lobe in primary stages, although here a diffuse pattern could be recognized. Also, the striatum and cerebellar white matter and dentate nucleus were involved in the first stages. The globus pallidus was involved in later stages as compared to the other two subgroups. Contrastingly to the other SuStaIn subgroups, the subthalamic nucleus showed (severe) tau tracer binding in later stages (Fig. 3C).

3.3. *Significant differences in regional tau accumulation patterns between the classical subcortical, the rhombencephalic and the cortical pattern*

SPM analysis of the DVR images showed no higher tau accumulation in subjects classified as the classical subcortical subtype when compared to subjects who were identified as the rhombencephalic subtype. When compared to the classical subcortical subtype, however, the cortical subtype had significantly higher cortical tau tracer binding. More specifically, involved cortical regions comprised the bilateral dorsolateral prefrontal cortex, primary motor cortex, premotor cortex, supplementary motor cortex and visual associative cortex. Furthermore, the left Broca operculum region, left supramarginal cortex, left visual motor cortex, the right secondary visual cortex, right inferior temporal gyrus, right primary somatosensory cortex and the cortical region known as the right frontal eye field showed higher tau tracer binding in the cortical subtype as compared to the classical subcortical subtype (Supplemental Table 1).

The rhombencephalic subtype showed higher tau binding in the subthalamic nucleus and the cerebellum bilaterally as compared to the classical subcortical subtype (Supplemental Table 1). When compared to the cortical subtype, patients in the rhombencephalic subtype showed higher tau tracer binding in the cerebellar vermis and the cerebellar crus on the left. Furthermore, cortical regions that showed higher tau tracer binding in the rhombencephalic subtype as compared to the cortical subtype were the bilateral frontal inferior operculum, right middle superior frontal gyrus, right rectus gyrus and left mid cingulate gyrus. The left hippocampus also showed higher tau binding in the rhombencephalic subtype as compared to the patients categorized as the cortical subtype.

When comparing the cortical subtype to the classical subcortical subtype, diffuse higher cortical tau tracer binding was observed (Fig. 4).

3.4. *Different SuStaIn-derived tau tracer binding patterns differ in demographic and clinical features*

A significant association between sex and SuStaIn subtype was noted (χ^2(df = 3) = 17198, P < 0.001, Cramér's V = 0.354). More particularly, males were more frequent in the classical subcortical subtype, females were more frequently represented in the rhombencephalic subtype, and a balanced male–female distribution was observed in the cortical subtype. The SuStaIn subtypes showed no significant differences in age of onset (F = 0.721; P = 0.489) or disease duration (H = 0.022; P = 0.989). No significant differences in cognitive functioning as assessed by the MoCA questionnaire were revealed between subgroups (H = 1.219; P = 0.544). Also, median SEADL score was not significantly different across the SuStaIn groups, although a tendency towards significance was noted (H = 5.409; P = 0.067). However, the PSP rating scale showed significantly different scores between the three subtypes (H = 6.796; P = 0.033). The rhombencephalic subtype individuals had the highest median PSP rating scale score. Using the chi-squared test, we found no significant correlation between the three SuStaIn subtypes and the frequency of the clinical phenotypes (e.g., PSP-RS, PSP-P, PSP-CBS) (χ^2(df = 12) = 18996, P = 0.089, Cramér's V = 0.304).

In the classical subcortical subtype, the SuStaIn-based tau PET staging was significantly correlated with the Kovacs-based PET staging (r = 0.40; P < 0.001).

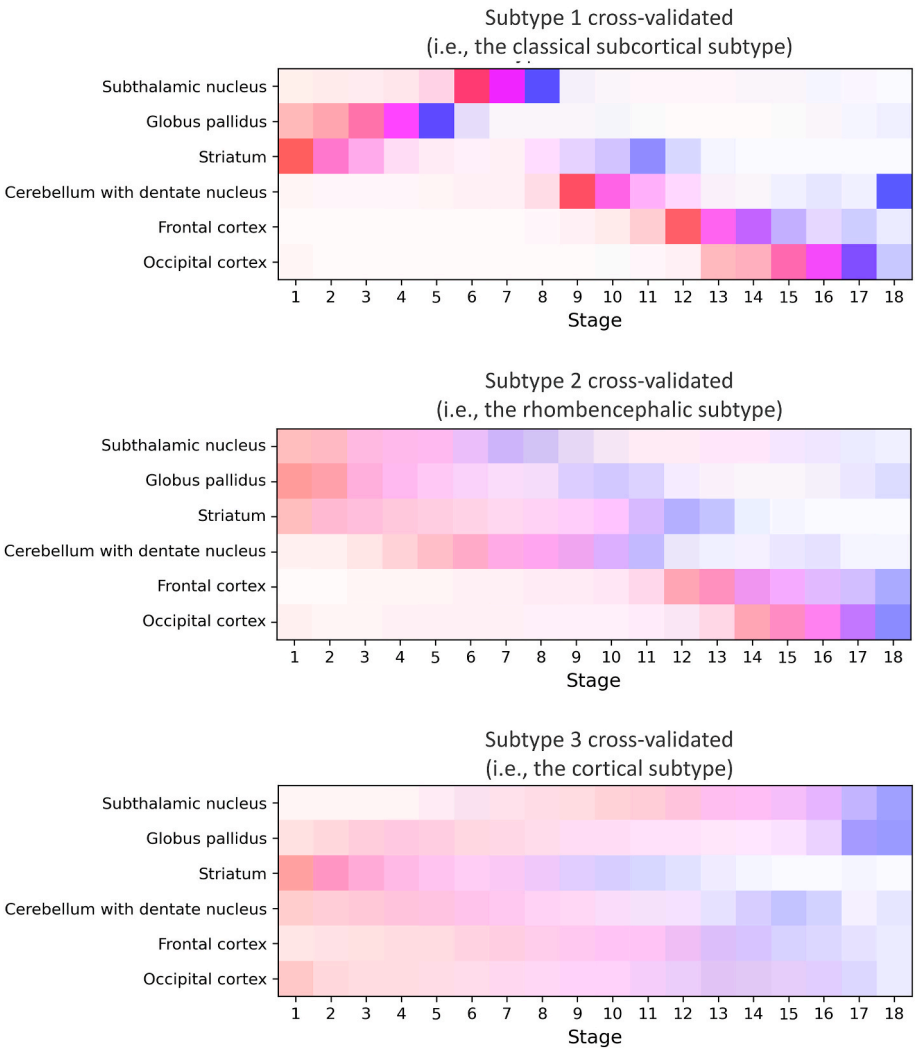

Fig. 3. Positional variance diagrams of each SuStaIn subtype showing the maximum likelihood event sequence. This diagram shows the cross-validated results of the positional variance diagram of the Markov Chain Monte Carlo samples for each subtype. Each entry represents the proportion of samples with each biomarker in each position ranging from 0 in white to 1 in red, magenta or blue. Cumulative probabilities corresponding to z-scores between 0 and 1 standard deviations (SD) were shown using a white-to-red color gradient. For z-scores between 1 and 2 SD, a white-to-magenta gradient was applied, and for z-scores between 2 and 3 SD, a white-to-blue gradient was used.

4. Discussion

Spatiotemporal clustering of [^{18}F]PI-2620 PET tracer binding images of PSP patients by use of the unsupervised machine learning algorithm SuStaIn provided three distinct subtypes. First, the classical subcortical subtype (SuStaIn subtype 1) was found, showing a distribution pattern similar to that described by Kovacs et al. [11]. In this SuStaIn subtype, most subjects were male. Furthermore, this subtype showed a significant correlation with the established postmortem PSP staging system [11] based on in vivo staging with [^{18}F]PI-2620 PET imaging. This suggests close alignment with known pathological staging. The second SuStaIn subtype showed to be a rhombencephalic subtype, included significantly more female subjects. Here, it was noted that patients had the highest median PSP rating scale score, indicating that this group was clinically more severely affected than the other groups. In the neuropathology staging scheme [11], a rostral and caudal type was identified in the 3rd and 4th stage that reflected the interindividual variability in the direction of progression as we show here in the PET. Despite involving subcortical areas also in early stages, based on the early cortical involvement, the third SuStaIn subtype showed to be a cortical subtype, and contained a balanced male–female distribution. Interestingly, the SuStaIn stage 0 subgroup, which we expected to purely represent healthy controls, also included up to 15% of all patients with a clinical diagnosis of PSP. This is in line with previous translational research in which one of the seven clinical evident cases of PSP displayed only limited tau accumulation as measured by both [^{18}F]PI-2620 signal and histopathological staining methods [24]. More research is needed to elucidate how this clinical–pathological discrepancy arises.

4.1. Potential prospects for in vivo PSP tau pathology staging by use of [^{18}F]PI-2620

Tau PET imaging, especially when using second-generation tracers, have been shown to be capable to distinguish PSP patients from healthy subjects [7]. More specifically, the use of [^{18}F]PI-2620, especially when combined with structural MRI data, has been found capable to provide higher diagnostic accuracy to identify PSP patients [25]. Present research findings corroborate that, in a subgroup of PSP patients, [^{18}F]PI-2620 PET imaging is capable of in vivo staging following the histopathological staging system [11]. This is mostly compatible with the classical subcortical subtype, which represents the largest amount of cases and the SuStaIn-derived disease stages in this subgroup significantly correlated with literature-derived histopathological disease stages. Importantly, the pattern described here as the rhombencephalic

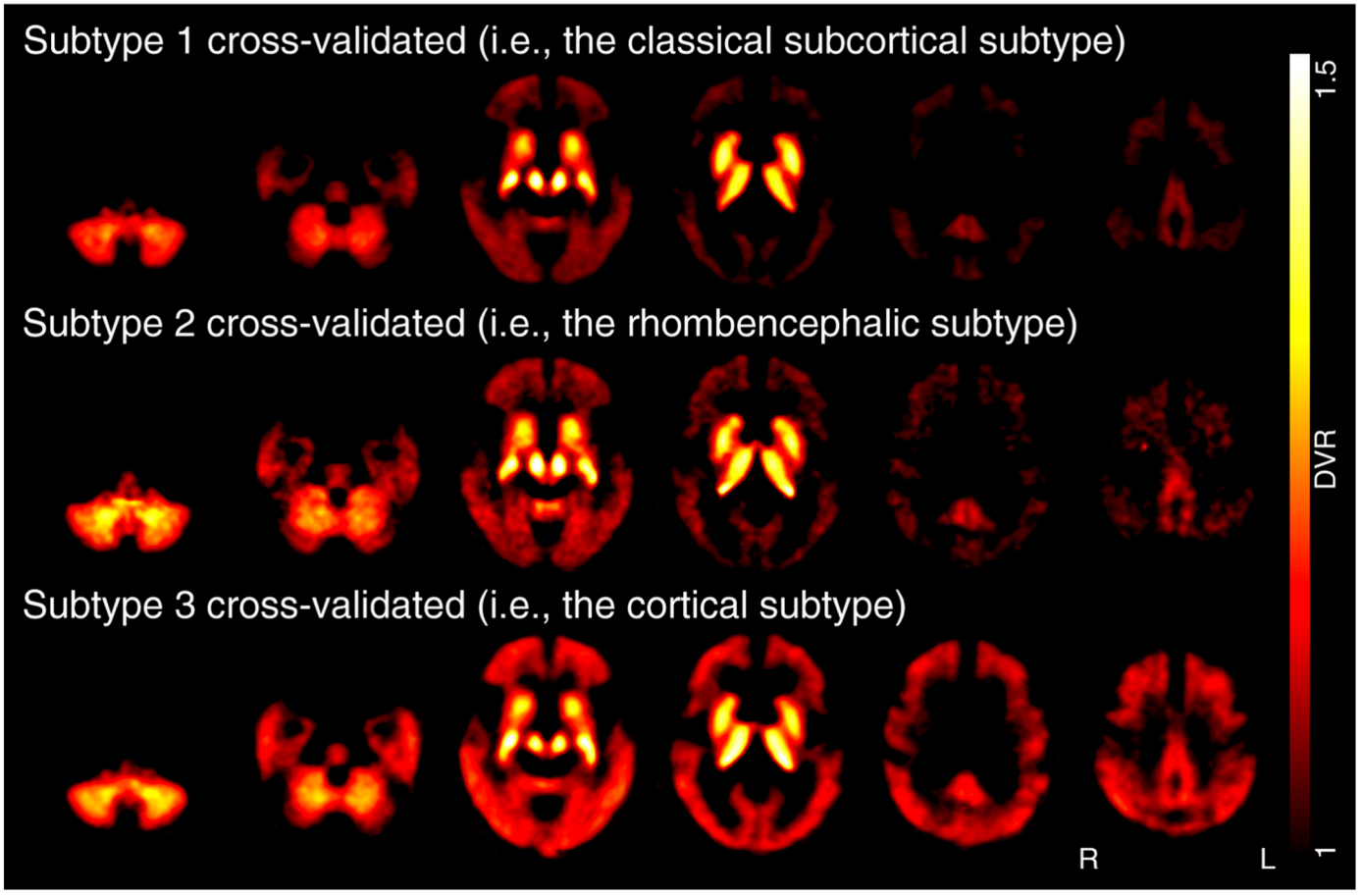

Fig. 4. Overview of [^{18}F] PI2620 tau PET tracer binding patterns in the three SuStaIn derived subtypes. Axial slices of averaged DVR maps for each subtype are shown. It can be appreciated that SuStaIn subtype 1 (n = 62) shows intense tau tracer binding in the region of the subthalamic nucleus, globus pallidus and striatum. Less pronounced is the tau tracer binding at the level of the dentate nucleus. Only limited cortical tau tracer binding in frontal and occipital regions can be observed. On the contrary, the cerebellar white matter and dentate nucleus shows intense tau tracer binding in SuStaIn subtype 2 (n = 24). Similar to SuStaIn subtype 1, intense tau tracer binding in the region of the subthalamic nucleus, globus pallidus and striatum can be appreciated in SuStaIn subtype 2. In SuStaIn subtype 3 (n = 17), a moderate intense tau tracer binding in the cortex can be observed, which is clearly different from cortical tau tracer binding in the other two SuStaIn derived subtypes. DVR: Distribution Volume Ratio; R: right; L: left.

subtype is also mentioned in the neuropathology staging system [11]. Others, however, found that tau PET imaging was not able to accurately stage PSP patients [26], although an in-depth comparison of results is hampered by difference in sample size, used radiopharmaceuticals (first generation tau PET tracers vs. second generation tau PET tracers) and study design. It could, however, be hypothesized that in the study of Malpetti et al., the correlation statistics were disturbed by inclusion of subjects with a different spatiotemporal subtype of PSP (i.e., rhombencephalic and cortical subtypes). Furthermore, histopathological validation of a small sample of patients (n = 9) showed that 89% of cases was staged lower or equal by PET as compared to histopathological validation. However, it must be noted that the mean duration between in vivo PET staging and ex vivo validation ranged between 0.5 and 4.0 years and progression of the disease over time in these subjects can therefore not be excluded [26]. Therefore, more research is needed on the post-mortem validation of in vivo tau tracer binding in a subtype of patients with a subcortical tau tracer binding pattern. Regarding the cortical subtype, it must be stated that this pattern could be partially explained by the fact that tau positivity can be observed in various individuals. Recently, Ossenkoppele et al. reported on their analysis of 42 cohorts (n = 12,048), including 7394 cognitively unimpaired participants, 2177 participants with mild cognitive impairment and 2477 participants with dementia. They reported that from age 60 years to 80 years, tau PET positivity in a temporal composite region increased from 1.1% to 4.4% among cognitive unimpaired, amyloid-β-negative participants and from 17.4% to 22.2% among cognitive unimpaired, amyloid-β-positive participants [27]. Although the amyloid-β-status of the study participants is not known in the current study, based on the aforementioned numbers it cannot be ruled out that the cortical subtype is partially explained by cortical tau as a normal aging phenomenon.

4.2. *Three SuStaIn subtypes vs. two SuStaIn subtypes*

One previous study investigated the use of the SuStaIn algorithm to spatiotemporally classify tau PET images of the brains of patients with PSP. In this study by Hong et al., two SuStaIn subtypes were described. Patients classified as SuStaIn Subtype 1 by Hong et al. typically exhibited a progression of tau tracer binding, starting at subcortical structures and gradually involving the cortical regions. Patients belonging to SuStaIn Subtype 2 by Hong et al. were characterized by an early, simultaneous onset in both cortical and subcortical regions [10]. Despite using a different radiotracer (i.e., [^{18}F]Florzolotau vs. [^{18}F] PI-2620) and different regions of interest as compared to the study of Hong et al., we also found a clear cortical subtype by use of the SuStaIn algorithm. Different from Hong et al., we attempted to validate our findings by use of statistical parametric mapping. This provided more insights in the distinct patterns that can be appreciated on [^{18}F]PI-2620 PET images of patients suffering from PSP. Furthermore, a third subtype was found in the present study. Based on the SuStaIn guidelines, the optimal number of subtypes that could be recognized by SuStaIn based

on the input data of the present study, was different from the number of subtypes reported in the study of Hong et al. [10]. This might be explained by the fact that we used less regions of interest. This was the case as we used a deductive hypothesis that was based on histopathological evidence of patterns of tau tracer binding in PSP patients [11]. Although we performed no further functional MRI investigations, the study of Hong and colleagues showed that SuStaIn subtype 2 displayed a remarkable reduction in functional connectivity compared to SuStaIn subtype 1. This could be in line with the cascading network failure theory [28,29], in which tau tracer binding in highly connected brain regions is associated with rapid local and widespread network failure. Although mainly described in Alzheimer's disease, our group previously reported this phenomenon in PSP patients [30].

4.3. Imaging-derived PSP tau pathology subtypes vs. clinical phenotype

In agreement with the study of Hong et al. [10], we also found differences in patient characteristics between the different SuStaIn subtypes. In the study of Hong et al., patients who were categorized as Subtype 2 were generally older and exhibited less severe dysfunctions in areas such as cognition, bulbar, limb motor, and general motor functions compared to those with Subtype 1. Moreover, they seemed to have a more favorable prognosis in terms of limb motor function and significant correlations between clinical variables (e.g., PSP rating scale, Movement Disorder Society Unified Parkinson's Disease Rating Scale III) and the identified PSP SuStaIn stages were found [10]. Although we found no significant correlation between SuStaIn subtypes and clinical phenotypes of PSP, another study reported that the regional tracer binding of [^{18}F]PI-2620 on PET images correlated with clinical symptoms. For example, patients with clinical signs of disorientation and bradyphrenia showed tracer uptake in the parieto-occipital junction, whereas the clinical signs disorientation and arising from chair were negatively correlated with tau PET signal in the caudate nucleus and thalamus [31]. However, discussion with regard to the diagnostic criteria of different PSP phenotypes exists. For example, a recent report showed that when applying the diagnostic criteria on PSP patients, nearly all patients (92.6%; 240 out of 259) were classified as PSP-RS patients. Furthermore, 60% (9 out of 15) of the PSP-P patients fulfilled both the criteria for PSP-RS and PSP-P [32]. Therefore, diagnostic accuracy of tau PET imaging to discern different PSP phenotypes might be hindered by variability in clinical diagnosis rather than by its own diagnostic capacities. Besides, inherently linked to the SuStaIn algorithm, the disease stages in the studied population were derived from cross-sectional data and could not be verified by longitudinal data.

4.4. Strengths and limitations

This study suffers from variable strengths and limitations. One particular strength of this study is the relatively large, multicenter cohort of clinically well-characterized PSP patients at baseline who were investigated with an extensive dynamic [^{18}F]PI-2620 PET imaging protocol. The use of [^{18}F]PI2620, a tau tracer with high affinity for 4R-tau pathology [4,9], strengthens the biological relevance of the findings. Moreover, the application of the SuStaIn algorithm enabled simultaneous modeling of phenotypical heterogeneity and disease stage, allowing identification of distinct spatiotemporal tau accumulation patterns rather than forcing patients into predefined clinical categories. Importantly, the SuStaIn-derived subcortical subtype showed a significant correlation with the established postmortem PSP tau staging system [11], supporting the construct validity of the imaging-based approach. Finally, the combination of region of interest analyses with voxel-wise statistical parametric mapping provided converging evidence for biologically meaningful subtype differences.

However, several limitations should also be acknowledged. The first concerns the use of the inferior cerebellar grey matter as a region of reference for intensity normalization, which is the common standard for [^{18}F]PI2620 PET assessment. However, this method has been developed for assessment of tau pathology in Alzheimer's disease, where the cerebellum typically shows little to no involvement [33]. In PSP, however, postmortem studies found that 4R tau accumulates in the cerebellar dentate nucleus and in oligodendrocytes in close vicinity to the cerebellar cortex [11]. Potentially, this confounds PET quantification. A recent study proposed the use of the temporo-orbital white matter as reference region [34]. However, this approach remains to be validated by others and, in order to improve comparability with other studies on the use of [^{18}F]PI2620 PET in PSP, we opted to use the common standard region for PET intensity normalization. Also, clinical follow-up duration and availability of demographic and clinical variables were heterogeneous, reflecting a real-world multicenter setting. This limited the ability to perform detailed longitudinal analyses or to fully explore temporal relationships between tau accumulation patterns and clinical progression. Importantly, the number of healthy controls was relatively small, which may have reduced the precision of z-score–based thresholding and limited sensitivity for detecting subtle early tau abnormalities. Nevertheless, all healthy controls underwent deep clinical phenotyping to rule out neurodegenerative changes by life. Additionally, 10/16 healthy controls underwent postmortem autoradiography, showing no [^{18}F]PI2620 binding.

Although we adjusted for center effects and observed that subtypes were distributed across multiple sites, residual scanner- or site-related variability cannot be fully excluded since full scanner harmonization across sites was not performed. Differences in PET hardware and reconstruction algorithms may therefore have introduced residual variability that could influence quantitative tracer uptake measures. Furthermore, PET images were normalized to MNI space using T1-weighted MRI when available and otherwise using early-phase PET images. While both approaches are valid, applying them interchangeably within the same dataset may introduce additional variability that could have influenced the outcomes of the here presented analyses. Additional analyses, excluding patients from whom no MRI was available, were performed. The positional variance diagram resulting from these separate analyses showed similar patterns with three similar subtypes (provided as Supplementary Fig. 1). Thereby, we concluded that the impact of these different normalization approaches within this database had no significant effect on the outcomes of the here presented study. SuStaIn modeling was based on cross-sectional data, and inferred disease stages could not be directly validated by longitudinal imaging within individuals. Finally, the observed cortical subtype recognized by SuStaIn could, in theory, represent patients suffering from Alzheimer's disease. Although clinical phenotypes were very uncharacteristic for that diagnosis, it cannot be ruled out completely that this could (partially) explain these imaging findings since the Amyloid-beta was unknown. Finally, the Tau PET PSP staging methodology was constructed as an in-vivo proxy of the study by Kovacs et al. [11] where, for each participant, regions corresponding to the different pathological stages were assessed and a stage was assigned based on the degree of tracer uptake across these regions. In order to degree the tracer uptake across regions, we stratified at thresholds of $z = 1$ (+, limited), $z = 2$ (++, mild), and $z = 3$ (+++, moderate/severe). These thresholds were used to approximate increasing levels of regional involvement, but do not constitute direct histopathological evaluations.

5. Conclusion

This study shows that the SuStaIn model is capable of distinguishing three subtypes of PSP based on [^{18}F]PI2620 PET data. Statistical parametric mapping showed that these subtypes elicited significantly different regional tau accumulation patterns: a subcortical subtype, a rhombencephalic subtype and a cortical subtype. More research is needed to warrant the here presented findings of different tau PET imaging-based subtypes of PSP and how these subtypes correlate with clinical phenotypes and symptomatology.

6. Key points

QUESTION: Can [^{18}F]PI2620 PET imaging, combined with a subtype/stage inference algorithm, identify patterns of tau buildup in progressive supranuclear palsy?

PERTINENT FINDINGS: Multicenter data showed distinct progressive supranuclear palsy tau subtypes and stages that aligned with clinical features, supporting robust in vivo disease characterization.

IMPLICATIONS FOR PATIENT CARE: This approach could enable earlier, more accurate diagnosis and staging of progressive supranuclear palsy, guide prognosis, and support tailored treatment strategies and clinical trial design.

Disclosure

Johannes Levin reports speaker fees from Bayer Vital, Biogen, EISAI, TEVA, Lilly, Zambon, Esteve, Merck and Roche, consulting fees from Axon Neuroscience, EISAI and Biogen, author fees from Thieme medical publishers and W. Kohlhammer GmbH medical publishers and is inventor in a patent "Oral Phenylbutyrate for Treatment of Human 4-Repeat Tauopathies" (PCT/EP2024/053388) filed by LMU Munich. In addition, he reports compensation for serving as chief medical officer for MODAG GmbH, is beneficiary of the phantom share program of MODAG GmbH and is inventor in a patent "Pharmaceutical Composition and Methods of Use" (EP 22,159,408.8) filed by MODAG GmbH, all activities outside the submitted work.

Guenter U. Hoeglinger has ongoing research collaborations with Roche, UCB, Abbvie; serves as a consultant for Abbvie, Alzprotect, Amylyx, Aprinoia, Asceneuron, Bayer, Bial, Biogen, Biohaven, Epidarex, Ferrer, Kyowa Kirin, Lundbeck, Novartis, Retrotope, Roche, Sanofi, Servier, Takeda, Teva, UCB; received honoraria for scientific presentations from Abbvie, Bayer, Bial, Biogen, Bristol Myers Squibb, Esteve, Kyowa Kirin, Pfizer, Roche, Teva, UCB, Zambon.

Gabor Kovacs reports personal fees from Parexel and Mitsubishi-Tanabe; funding from Rossy Family Foundation, from Edmond Safra Foundation, grants from Krembil Foundation, MSA Coalition, MJ Fox Foundation, Parkinson Canada, NIH, Canada Foundation for Innovation, and Ontario Research Fund outside the submitted work; in addition, GGK has a shared patent for 5G4 Synuclein antibody and a pending patent for Diagnostic assays for movement disorders (18/537,455), and received royalties from Wiley, Cambridge, Taylor and Francis, and Elsevier publishers.

Matthias Brendel is a member of the Neuroimaging Committee of the EANM. MB has received speaker honoraria from Roche, GE Healthcare, and Life Molecular Imaging; has advised Life Molecular Imaging; and is currently on the advisory board of MIAC.

Andre Mueller and Andrew W. Stephens are full-time employees at Life Molecular Imaging.

All the other authors declare that no conflicts of interest exist.

CRediT authorship contribution statement

Michael Rullmann: Conceptualization, Data curation, Formal analysis, Investigation, Methodology, Project administration, Visualization, Writing – original draft, Writing – review & editing. **Dylan Henssen:** Conceptualization, Data curation, Formal analysis, Investigation, Methodology, Project administration, Visualization, Writing – original draft, Writing – review & editing. **Matthias Brendel:** Conceptualization, Data curation, Formal analysis, Investigation, Methodology, Writing – original draft, Writing – review & editing. **Jost-Julian Rumpf:** Data curation, Formal analysis, Writing – review & editing. **Johannes Levin:** Data curation, Formal analysis, Writing – review & editing. **Robert Perneczky:** Data curation, Formal analysis, Writing – review & editing. **Solveig Tiepolt:** Data curation, Formal analysis, Writing – review & editing. **Marianne Patt:** Data curation, Formal analysis, Writing – review & editing. **Andreas Schildan:** Data curation, Formal analysis, Writing – review & editing. **Andre Mueller:** Data curation, Formal analysis, Writing – review & editing. **Victor L. Villemagne:** Data curation, Formal analysis, Writing – review & editing. **Joseph Classen:** Data curation, Formal analysis, Writing – review & editing. **Andrew W. Stephens:** Data curation, Formal analysis, Writing – review & editing. **Stamatia Karagianni:** Data curation, Formal analysis, Writing – review & editing. **Nicolai Franzmeier:** Data curation, Formal analysis, Writing – review & editing. **Gabor G. Kovacs:** Data curation, Formal analysis, Writing – review & editing. **Guenter U. Hoeglinger:** Data curation, Formal analysis, Writing – review & editing. **Osama Sabri:** Conceptualization, Data curation, Formal analysis, Investigation, Project administration, Resources, Writing – original draft, Writing – review & editing. **Henryk Barthel:** Conceptualization, Data curation, Formal analysis, Investigation, Project administration, Writing – original draft, Writing – review & editing.

Acknowledgements

Computations for this work were done (in part) using resources of the Leipzig University Computing Center. Dylan Henssen is supported by the, Clinician Scientist ProgrammUniversitätsmedizin Leipzig, which facilitates the integration of clinical practice and scientific research. Guenter U. Hoeglinger was funded by the Deutsche Forschungsgemeinschaft (DFG, German Research Foundation) under Germany's Excellence Strategy within the framework of the Munich Cluster for Systems Neurology (EXC 2145 SyNergy – ID 390857198).

Appendix A. Supplementary data

Supplementary data to this article can be found online at https://doi.org/10.1016/j.eanmj.2026.100226.

Data availability

Data will be made available on request.

References

[1] Rosler TW, Tayaranian Marvian A, Brendel M, Nykanen NP, Hollerhage M, Schwarz SC, et al. Four-repeat tauopathies. Prog Neurobiol 2019;180:101644.
[2] Stamelou M, Respondek G, Giagkou N, Whitwell JL, Kovacs GG, Hoglinger GU. Evolving concepts in progressive supranuclear palsy and other 4-repeat tauopathies. Nat Rev Neurol 2021;17(10):601–20.
[3] Respondek G, Hoglinger GU. The phenotypic spectrum of progressive supranuclear palsy. Parkinsonism Relat Disord 2016;22(Suppl 1):S34–6.
[4] Brendel M, Barthel H, van Eimeren T, Marek K, Beyer L, Song M, et al. Assessment of 18F-PI-2620 as a biomarker in progressive supranuclear palsy. JAMA Neurol 2020;77(11):1408–19.
[5] Li L, Liu FT, Li M, Lu JY, Sun YM, Liang X, et al. Clinical utility of (18) F-APN-1607 tau PET imaging in patients with progressive supranuclear palsy. Mov Disord 2021;36(10):2314–23.
[6] Liu FT, Lu JY, Li XY, Liang XN, Jiao FY, Ge JJ, et al. (18)F-Florzolotau PET imaging captures the distribution patterns and regional vulnerability of tau pathology in progressive supranuclear palsy. Eur J Nucl Med Mol Imag 2023;50(5):1395–405.
[7] Jin J, Su D, Zhang J, Li X, Feng T. Tau PET imaging in progressive supranuclear palsy: a systematic review and meta-analysis. J Neurol 2023;270(5):2451–67.
[8] Young AL, Marinescu RV, Oxtoby NP, Bocchetta M, Yong K, Firth NC, et al. Uncovering the heterogeneity and temporal complexity of neurodegenerative diseases with subtype and stage inference. Nat Commun 2018;9(1):4273.
[9] Bischof GN, Brendel M, Barthel H, Theis H, Barbe M, Bartenstein P, et al. Improved tau PET SUVR quantification in 4-Repeat tau phenotypes with [(18)F]PI-2620. J Nucl Med 2024;65(6):952–5.
[10] Hong J, Lu J, Liu F, Wang M, Li X, Clement C, et al. Uncovering distinct progression patterns of tau deposition in progressive supranuclear palsy using [(18)F] Florzolotau PET imaging and subtype/stage inference algorithm. EBioMedicine 2023;97:104835.
[11] Kovacs GG, Lukic MJ, Irwin DJ, Arzberger T, Respondek G, Lee EB, et al. Distribution patterns of tau pathology in progressive supranuclear palsy. Acta Neuropathol 2020;140(2):99–119.
[12] Hoglinger GU, Respondek G, Stamelou M, Kurz C, Josephs KA, Lang AE, et al. Clinical diagnosis of progressive supranuclear palsy: the movement disorder society criteria. Mov Disord 2017;32(6):853–64.
[13] Golbe LI, Ohman-Strickland PA. A clinical rating scale for progressive supranuclear palsy. Brain 2007;130(Pt 6):1552–65.

[14] Schwab RS, editor. Projection technique for evaluating surgery in parkinson's disease. Third symposium on parkinson's disease. E&S Livingstone; 1969.
[15] Nasreddine ZS, Phillips NA, Bedirian V, Charbonneau S, Whitehead V, Collin I, et al. The Montreal cognitive assessment, MoCA: a brief screening tool for mild cognitive impairment. J Am Geriatr Soc 2005;53(4):695–9.
[16] Beyer L, Nitschmann A, Barthel H, van Eimeren T, Unterrainer M, Sauerbeck J, et al. Early-phase [(18)F]PI-2620 tau-PET imaging as a surrogate marker of neuronal injury. Eur J Nucl Med Mol Imag 2020;47(12):2911–22.
[17] Ichise M, Liow JS, Lu JQ, Takano A, Model K, Toyama H, et al. Linearized reference tissue parametric imaging methods: application to [11C]DASB positron emission tomography studies of the serotonin transporter in human brain. J Cereb Blood Flow Metab 2003;23(9):1096–112.
[18] Diedrichsen J, Balsters JH, Flavell J, Cussans E, Ramnani N. A probabilistic MR atlas of the human cerebellum. Neuroimage 2009;46(1):39–46.
[19] Keuken MC, Forstmann BU. A probabilistic atlas of the basal ganglia using 7 T MRI. Data Brief 2015;4:577–82.
[20] Tzourio-Mazoyer N, Landeau B, Papathanassiou D, Crivello F, Etard O, Delcroix N, et al. Automated anatomical labeling of activations in SPM using a macroscopic anatomical parcellation of the MNI MRI single-subject brain. Neuroimage 2002;15(1):273–89.
[21] Briggs M, Allinson KSJ, Malpetti M, Spillantini MG, Rowe JB, Kaalund SS. Validation of the new pathology staging system for progressive supranuclear palsy. Acta Neuropathol 2021;141(5):787–9.
[22] Archetti D, Young AL, Oxtoby NP, Ferreira D, Martensson G, Westman E, et al. Inter-cohort validation of SuStaIn model for Alzheimer's disease. Front Big Data 2021;4:661110.
[23] Aksman LM, Wijeratne PA, Oxtoby NP, Eshaghi A, Shand C, Altmann A, et al. pySuStaIn: a python implementation of the subtype and stage inference algorithm. SoftwareX 2021;16.
[24] Slemann L, Gnorich J, Hummel S, Bartos LM, Klaus C, Kling A, et al. Neuronal and oligodendroglial, but not astroglial, tau translates to in vivo tau PET signals in individuals with primary tauopathies. Acta Neuropathol 2024;148(1):70.
[25] Messerschmidt K, Barthel H, Brendel M, Scherlach C, Hoffmann KT, Rauchmann BS, et al. (18)F-PI-2620 Tau PET improves the imaging diagnosis of progressive supranuclear palsy. J Nucl Med 2022;63(11):1754–60.
[26] Malpetti M, Kaalund SS, Tsvetanov KA, Rittman T, Briggs M, Allinson KSJ, et al. In vivo (18)F-Flortaucipir PET does not accurately support the staging of progressive supranuclear palsy. J Nucl Med 2022;63(7):1052–7.
[27] Ossenkoppele R, Coomans EM, Apostolova LG, Baker SL, Barthel H, Beach TG, et al. Tau PET positivity in individuals with and without cognitive impairment varies with age, amyloid-β status, APOE genotype and sex. Nat Neurosci 2025;28(8):1610–21.
[28] Jones DT, Knopman DS, Gunter JL, Graff-Radford J, Vemuri P, Boeve BF, et al. Cascading network failure across the Alzheimer's disease spectrum. Brain 2016;139(Pt 2):547–62.
[29] Jones DT, Graff-Radford J, Lowe VJ, Wiste HJ, Gunter JL, Senjem ML, et al. Tau, amyloid, and cascading network failure across the Alzheimer's disease spectrum. Cortex 2017;97:143–59.
[30] Aghakhanyan G, Rullmann M, Rumpf J, Schroeter ML, Scherlach C, Patt M, et al. Interplay of tau and functional network connectivity in progressive supranuclear palsy: a [(18)F]PI-2620 PET/MRI study. Eur J Nucl Med Mol Imag 2022;50(1):103–14.
[31] Schonecker S, Palleis C, Franzmeier N, Katzdobler S, Ferschmann C, Schuster S, et al. Symptomatology in 4-repeat tauopathies is associated with data-driven topology of [(18)F]-PI-2620 tau-PET signal. Neuroimage, Clin 2023;38:103402.
[32] Shoeibi A, Litvan I, Juncos JL, Bordelon Y, Riley D, Standaert D, et al. Are the International Parkinson disease and movement disorder society progressive supranuclear palsy (IPMDS-PSP) diagnostic criteria accurate enough to differentiate common PSP phenotypes? Parkinsonism Relat Disord 2019;69:34–9.
[33] Braak H, Braak E. Neuropathological stageing of alzheimer-related changes. Acta Neuropathol 1991;82(4):239–59.
[34] Frontzkowski L, Gnorich J, Gross M, Dehsarvi A, Roemer-Cassiano SN, Palleis C, et al. Developing a novel reference region for [(18)F]PI-2620-PET imaging to facilitate the assessment of 4-repeat tauopathies. Eur J Nucl Med Mol Imag 2025;52(13):5098–112.